Progress In Electromagnetics Research C, Vol. 32, 81–94, 2012

RANDOM STEP FREQUENCY CSAR IMAGING BASED ON COMPRESSIVE SENSING

L. Yu[1, 2, *] and Y. Zhang[2]

[1]Jiangxi University of Science and Technology, Ganzhou 341000, China

[2]The Key Laboratory of Microwave Remote Sensing, Chinese Academy of Sciences, Beijing 100190, China

Abstract—Circular synthetic aperture radar (CSAR) imaging based on compressive sensing with random step frequency (RSF) as transmitted signal is introduced. CSAR is capable of obtaining both two-dimensional high resolution image and three-dimensional image due to a circular collection trajectory. RSF signal shares good characteristics of noise signals including "thumbtack-shape" ambiguity function, low probability of interception, and strong anti-jamming capability. As a result, CSAR adopting RSF signal can make use of advantages of both CSAR and RSF signal. Compressive sensing is a new data acquisition and reconstruction theorem for sparse or compressible signals, which needs fewer samples to reconstruct signals than traditional Nyquist theorem. Simulation results show that both two-dimensional and three-dimensional targets can be well reconstructed from few samples by applying compressive sensing to RSF CSAR imaging.

1. INTRODUCTION

In circular synthetic aperture radar (CSAR), both two-dimensional (2D) high resolution image and three-dimensional (3D) image of targets can be obtained because of the complete 360 degree synthetic aperture. At present, CSAR has been widely used in automatic target recognition (ATR) system for tank or vehicles [1–3], high resolution imaging of building or urban area [4–7], detection of targets in the foliage or under the ground [8], and detection of concealed objects in airport security systems [9, 10].

Received 15 June 2012, Accepted 9 August 2012, Scheduled 14 August 2012

* Corresponding author: Lingjuan Yu (yljsmile@163.com).

It is known that the random step frequency (RSF) signal, as one of random noise signals, has "thumbtack-shape" ambiguity function of low sidelobe and high resolution in range-Doppler domain, low probability of interception, and strong anti-jamming capability [11, 12]. Axelsson analyzed that transmitting randomly changed frequencies could suppress range ambiguity, improve covert detection, and reduce signal interference between adjacent sensors [12]. It is obvious that if RSF signal is used as the transmitting signal in CSAR system, one can combine the advantage of CSAR with that of random signals.

Compressive sensing (CS), which is different from the traditional Nyquist theorem, has been presented for sparse or compressible signals recently [13–15]. So far, CS theorem has been widely used in the signal processing of SAR [16–20]. Lin et al. applied CS to CSAR imaging, aiming to reduce the number of samples and provide high image quality [21]. In this paper, we apply CS to RSF CSAR imaging of both 2D and 3D targets.

The rest of this paper is organized as follows. The echo model of random step frequency CSAR is discussed in Section 2. The important content about compressive sensing is briefly introduced in Section 3. The principle of random step frequency CSAR imaging based on CS is illustrated in Section 4, and simulation results of 2D and 3D targets are given in Section 5. Finally, Section 6 contains conclusions.

2. THE ECHO MODEL OF RANDOM STEP FREQUENCY CSAR

The CSAR imaging geometry is shown in Fig. 1(a). Its top view and side view are shown in Figs. 1(b) and (c), respectively. Let's denote

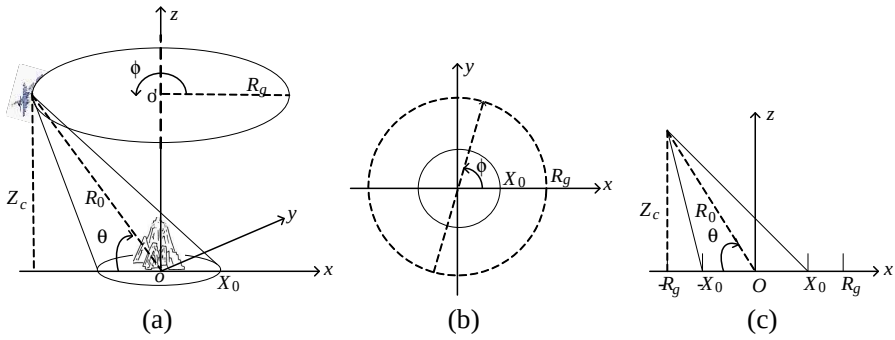

Figure 1. (a) Geometry of CSAR imaging system. (b) Top view. (c) Side view.

the radar height as z_c, and the flight radius as R_g. Then the slant range can be expressed as,

$$R_0 = \sqrt{R_g^2 + z_c^2} \tag{1}$$

and the slant depression angle can be calculated by

$$\theta = \arctan\left(\frac{z_c}{R_g}\right) \tag{2}$$

In linear step frequency radar, the center frequency is f_c, and the frequency is stepped linearly with frequency step of Δf, i.e., the signal can be expressed as,

$$f_i = f_c + i \times \Delta f \tag{3}$$

where $i = -N_r/2, -N_r/2 + 1, \ldots N_r/2$, N_r is even, and $N_r + 1$ is the total frequency number.

In RSF radar, frequencies are not linearly increased, but are subjected to some random distribution. In order to simplify the model, uniform distribution is adopted. Assume i is subjected to uniform distribution over $[-N_r/2, N_r/2]$, and then the frequency is denoted as f_i'. If the discrete i is sorted by i', $i' = 1, 2 \ldots N_r, N_r + 1$, then the corresponding frequencies can be denoted as $f_1', f_2', \ldots f_{N_r}', f_{N_r+1}'$.

If there are P discrete 3D targets, the received echo signal of RSF CSAR shall be,

$$S\left(k', \phi\right) = \sum_{p=1}^{P} \sigma_p \exp\left\{-jk' R_p(\phi)\right\} \tag{4}$$

where $k' = 2\pi f'/c$ is wave number, c is light speed, $p = 1, 2, \ldots P$ is the index number of point targets, σ_p is radar cross section, and $R_p\left(\phi\right)$ is the slant range, which can be expressed as,

$$R_p\left(\phi\right) = \sqrt{(x_p - R_g \cos\phi)^2 + (y_p - R_g \sin\phi)^2 + (z_p - Z_c)^2} \tag{5}$$

where (x_p, y_p, z_p) is the 3D coordinates of the p-th target.

For 2D targets, the echo model can also expressed by Equation (4), and the target height is set to be zero, i.e., $z_p = 0$ in Equation (5).

3. COMPRESSIVE SENSING

CS is a new signal sampling and reconstructing theorem. It mainly includes three parts of sparse representation, incoherent measurement, and signal recovery. CS theory states that if a signal has a sparse representation in some basis, it can be approximately reconstructed

with acceptable accuracy by using only few measurements. In the following, one dimensional signal processing with CS will be described in detail.

Let's denote a real discrete signal of length N as x, which is sparse in basis $\mathbf{\Psi^T} = [\psi_1, \psi_2 \dots \boldsymbol{\psi_N}]$ where $\boldsymbol{\psi}_n$ $(n = 1, 2, \dots N)$ is a vector of same length N. It can be written as,

$$x_{N\times 1} = \mathbf{\Psi}_{N\times N}\alpha_{N\times 1} \tag{6}$$

where α are the corresponding coefficients of basis $\mathbf{\Psi}$ and have only $K \ll N$ nonzero values.

Assume the signal is projected to measurement basis $\mathbf{\Phi} = [\phi_1, \phi_2 \dots \phi_M]$, where ϕ_m $(m = 1, 2, \dots M)$ is a vector of length N, and the measurements can be written as,

$$y_{M\times 1} = \mathbf{\Phi}_{M\times N} x_{N\times 1} \tag{7}$$

By substituting Equation (6) into (7), we obtain,

$$y = \mathbf{\Phi} x = \mathbf{\Phi\Psi}\alpha = \mathbf{\Theta}\alpha \tag{8}$$

where $\mathbf{\Theta} = \mathbf{\Phi\Psi}$ and $K < M$.

If $\mathbf{\Theta}$ satisfies the restricted isometry property (RIP), or $\mathbf{\Phi}$ and $\mathbf{\Psi}$ are incoherent, α can be recovered through (8). This recovery can be implemented by solving an optimization problem with the minimum l_0-norm,

$$\min_{\alpha} \|\alpha\|_{l_0} \quad \text{such that } y = \mathbf{\Phi\Psi}\alpha \tag{9}$$

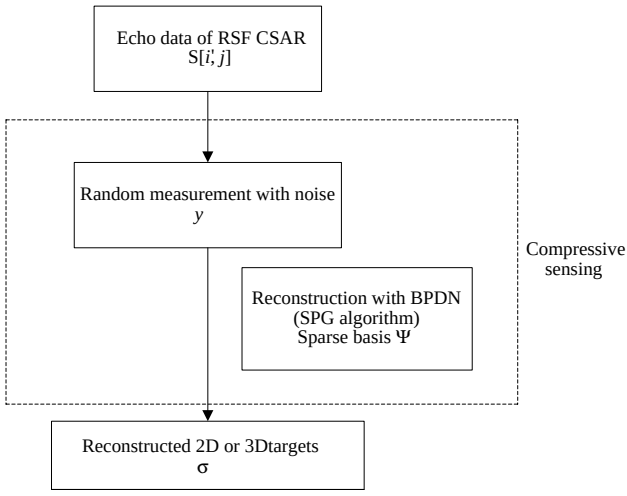

Figure 2. The procedure of RSF CSAR imaging based on CS.

Table 1. The system parameters.

Frequency range	[8 GHz, 12 GHz]
Radius of the flight track	200 m
Height locations of the radar	200 m
Radius of imaging area	0.2 m

Table 2. The original 2D point targets.

Scatter No.	(x, y) (m)	Amplitude	Scatter No.	(x, y) (m)	Amplitude
1	$(-0.1, -0.1)$	1	6	$(0, 0.1)$	1
2	$(-0.1, 0)$	1	7	$(0.1, -0.1)$	1
3	$(-0.1, 0.1)$	1	8	$(0.1, 0)$	1
4	$(0, -0.1)$	1	9	$(0.1, 0.1)$	1
5	$(0, 0)$	1			

Solving Equation (9) is NP-hard (non-deterministic polynomial-time hard). However, it can be equivalent to the minimum l_1-norm reconstruction,

$$\min_{\alpha} \|\alpha\|_{l_1} \quad \text{such that } y = \mathbf{\Phi\Psi}\alpha \tag{10}$$

There are many ways to solve (10). After obtaining α, signal x is also recovered through (6).

4. RANDOM STEP FREQUENCY CSAR IMAGING BASED ON CS

Because of the random waveform, the traditional back projection algorithm implemented by fast Fourier transform can not be used any more. In Section 2, the echo model of RSF CSAR is built up, and the frame of CS is introduced in Section 3. In this section, CS is applied to the imaging processing.

By dividing the 3D target scene into $M \times N \times L$ pixels, the received echo expressed by (4) can then be rewritten as,

$$S[i', j] = \sum_{l=1}^{L} \sum_{n=1}^{N} \sum_{m=1}^{M} \sigma_{mnl} \exp\{-jk_{i'} R_{mnl}(\phi_j)\} \tag{11}$$

where $R_{mnl}(\phi_j) = \sqrt{(x_{mnl} - R_g \cos\phi_j)^2 + (y_{mnl} - R_g \sin\phi_j)^2 + (z_{mnl} - Z_c)^2}$, $j = 1, 2 \ldots N_a$ and $i' = 1, 2 \ldots N_r, N_r + 1$. If no target falls in the pixel, then let $\sigma = 0$.

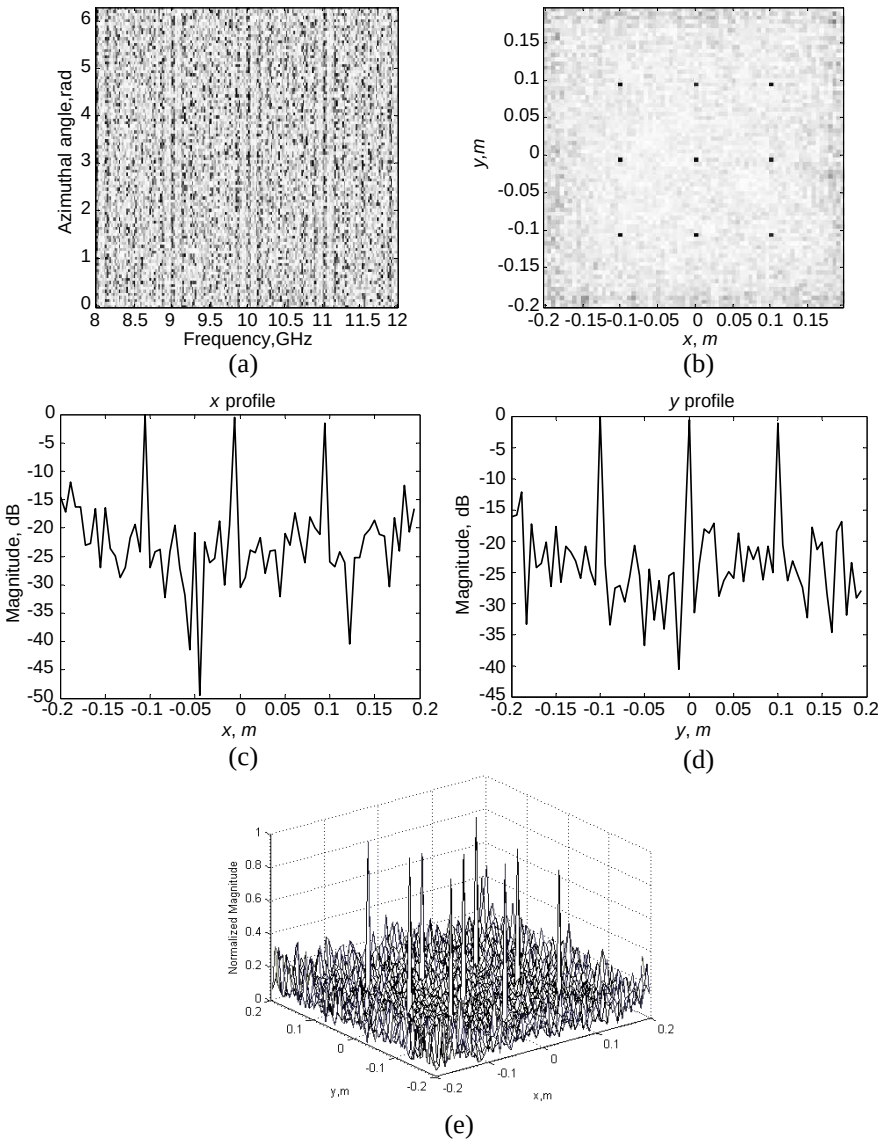

Figure 3. Nine 2D point targets (SNR = 20 dB). (a) Echo. (b) 2D imaging result. (c) x profile ($y = 0$). (d) y profile ($x = 0$). (e) 3D plot.

If the number of target is limited, coefficients σ will be sparse. We can further define the sparse basis as,

$$\boldsymbol{\psi}_{i'j}(x_{mnl}, y_{mnl}, z_{mnl}) = \exp\{-jk_{i'}R_{mnl}(\phi_j)\} \tag{12}$$

In practice, noise is unavoidable in measurements, so the measured

model should be modified as,

$$\mathbf{y} = \mathbf{\Phi}S + \mathbf{n} = \mathbf{\Phi\Psi}\boldsymbol{\sigma} + \mathbf{n} = \mathbf{\Theta}\sigma + \mathbf{n} \tag{13}$$

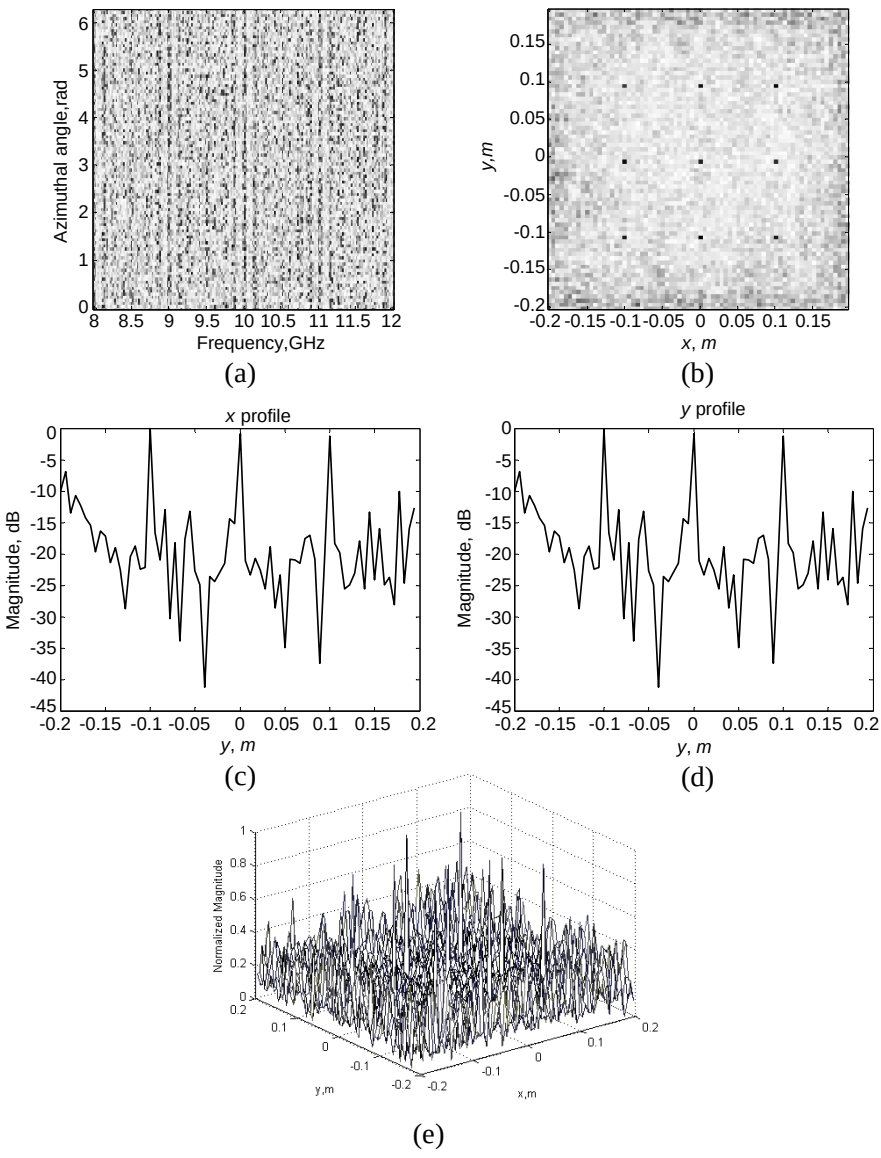

Figure 4. Nine 2D point targets (SNR = 15 dB). (a) Echo. (b) 2D imaging result. (c) x profile (y =0). (d) y profile ($x = 0$). (e) 3D plot.

where $\mathbf{y}$ is the measurement, $\mathbf{\Phi}$ is the measured matrix, and $\mathbf{n}$ is the noise.

Here (13) is solved by basis pursuit denoise (BPDN) [22],

$$\min_{\sigma} \|\sigma\|_{l_1} \quad \text{such that } \|\mathbf{y} - \mathbf{\Phi}\mathbf{\Psi}\boldsymbol{\sigma}\|_2 \leq \varepsilon \tag{14}$$

where $\varepsilon \geq 0$ is an estimate of the noise level.

If we choose $\mathbf{\Phi}$ to be a random matrix in (13), then the spectral projected gradient (SPG) algorithm [23] can be used to recover sparse coefficients σ through Equation (14). Because both sparse basis and measured matrix are random matrixes, it is easy to confine RIP condition. For 2D targets, we can just let $L = 1$, $z_{mnl} = 0$ in (11) and (12), respectively.

For both 3D and 2D targets, the above procedure of RSF CSAR imaging based on CS can be shown in Fig. 2.

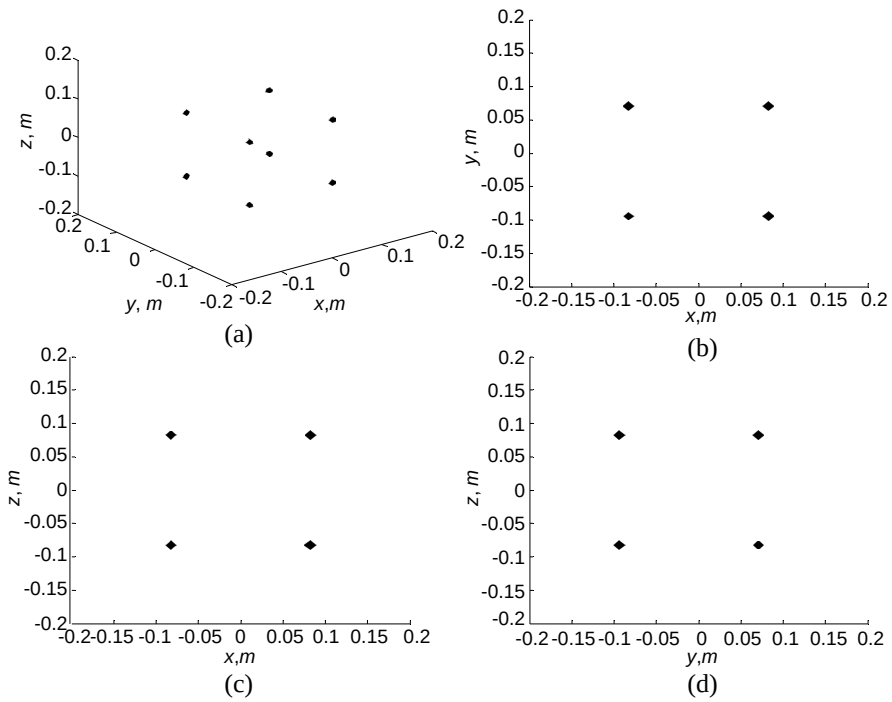

Figure 5. Imaging results of eight 3D point targets (SNR = 20 dB). (a) 3D imaging result. (b) Projection on xy plane. (c) Projection on xz plane. (d) Projection on yz plane.

5. SIMULATION RESULTS

In order to observe the imaging results of RSF CSAR based on CS, reconstructions of 2D and 3D point targets are simulated and presented, respectively. The system parameters are listed in Table 1.

5.1. 2D Point Targets

The original target coordinates and amplitude of nine 2D point targets are listed in Table 2. In simulation, zero-mean white Gaussian random noise is added to echo, and signal-to-noise ratio (SNR) is about 20 dB. Fig. 3(a) shows the amplitude of received echo. From Fig. 3(a) one can see that the echo is almost like noise, so it is hard to obtain any information without prior knowledge about the signal.

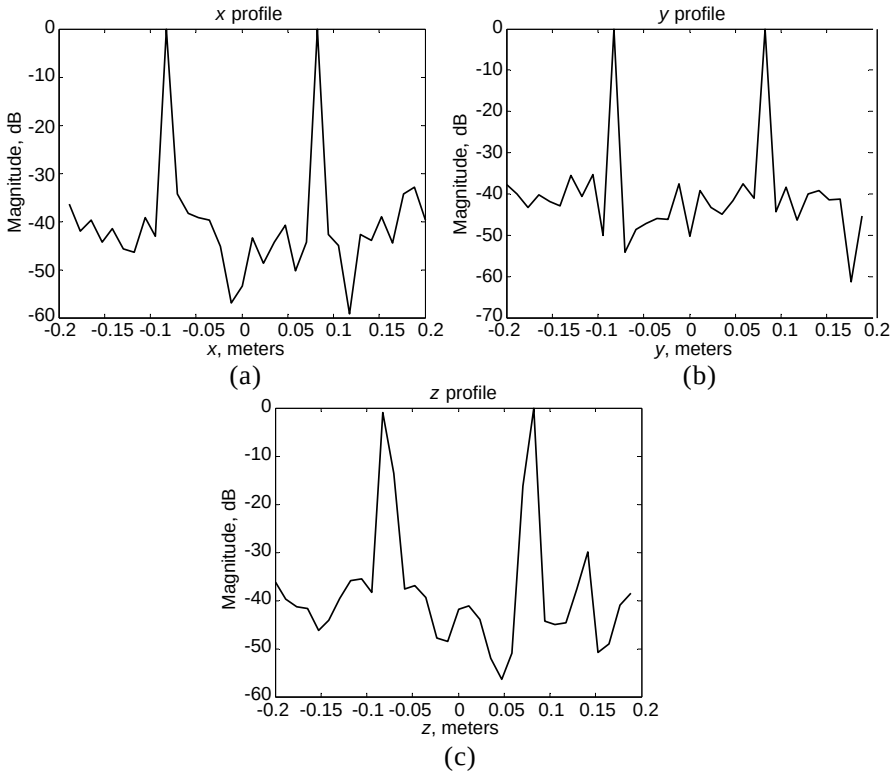

Figure 6. Imaged 3D point target profiles (SNR = 20 dB). (a) x profile ($y = 0.08$ m, $z = 0.08$ m). (b) y profile ($x = 0.08$ m, $z = 0.08$ m). (c) z profile ($x = 0.08$ m, $y = 0.08$ m).

The 2D imaging result with 10% random echo samples is shown in Fig. 3(b). The x ($y = 0$) and y ($x = 0$) profiles of Fig. 3(b) are shown in Figs. 3(c)–(d). The 3D plot of Fig. 3(b) is shown in Fig. 3(e). Figs. 3(b)–(e) clearly show that nine point targets are all well reconstructed.

In the following, we shall conduct another simulation for SNR = 15 dB. The corresponding results are shown in Figs. 4(a)–(e), from which one can see nine targets can also be reconstructed from few samples. After comparing Fig. 4 with Fig. 3, we can see that the sidelobes of reconstructed targets are increased when SNR is decreased.

5.2. 3D Point Targets

The original target coordinates and amplitude of eight 3D point targets are listed in Table 3. Zero-mean white Gaussian random noise is also

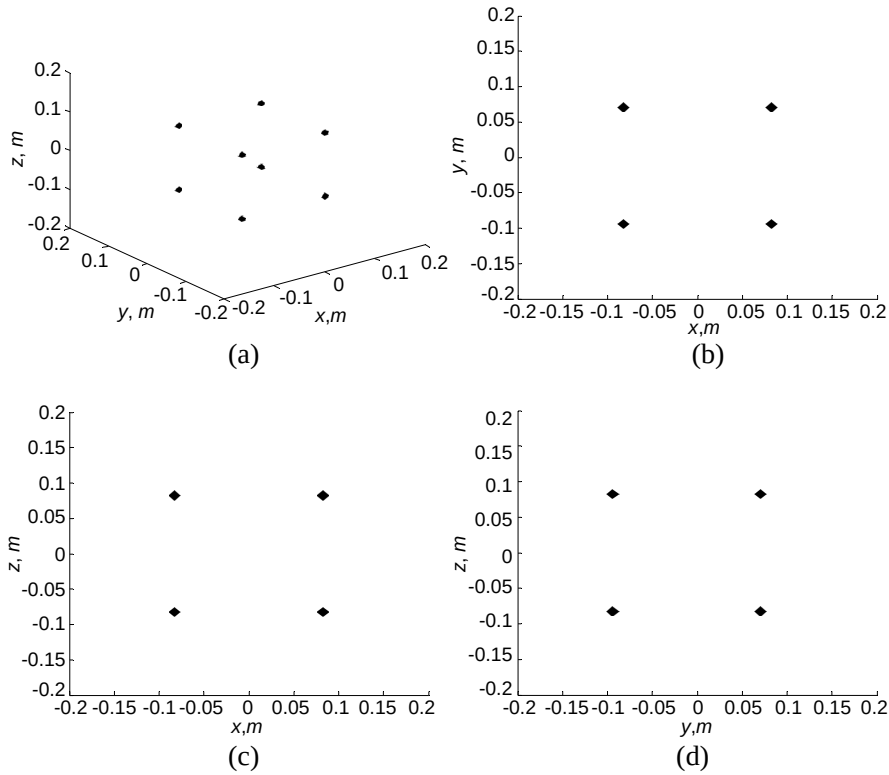

Figure 7. Imaging results of eight 3D point targets (SNR = 15 dB). (a) 3D imaging result. (b) Projection on xy plane. (c) Projection on xz plane. (d) Projection on yz plane.

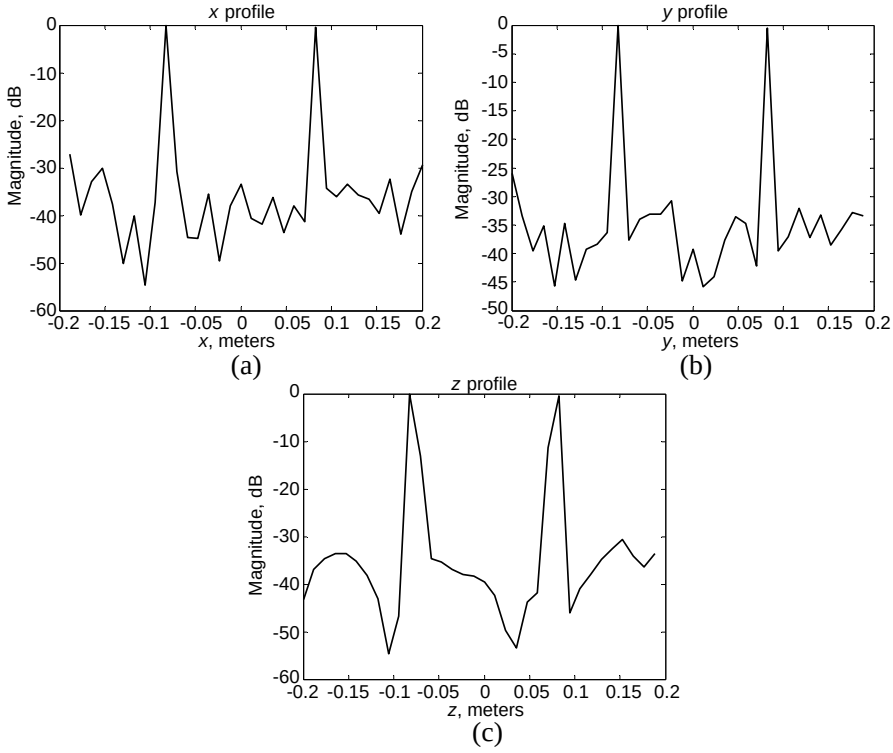

Figure 8. Imaged 3D point target profiles (SNR = 15 dB). (a) x profile ($y = 0.08$ m, $z = 0.08$ m). (b) y profile ($x = 0.08$ m, $z = 0.08$ m). (c) z profile ($x = 0.08$ m, $y = 0.08$ m).

added to the echo as above done, and SNR is about 20 dB.

The 3D imaging result with 10% random echo samples is shown in Fig. 5(a), and the projections on xy, xz, and yz planes are shown in Figs. 5(b)–(d), respectively. The x ($y = 0.08$ m, $z = 0.08$ m), y ($x = 0.08$ m, $z = 0.08$ m), and z ($x = 0.08$ m, $y = 0.08$ m) profiles of Fig. 5(a) are shown in Figs. 6(a)–(c), respectively.

All these figures are -6 dB contoured after amplitude normalized. The same as 2D point targets case, 3D point targets are also very well reconstructed from few samples.

Once again, simulations for SNR = 15 dB are conducted. The corresponding results are shown in Fig. 7 and Fig. 8, respectively, which also indicate that 3D point targets can be reconstructed. Comparing Fig. 7 with Fig. 5, -6 dB contoured figures are almost the same. But comparing Fig. 8 with Fig. 6, the sidelobes of one-dimensional profiles

Table 3. The original 3D point targets.

Scatter No.	(x, y, z) (m)	Amplitude	Scatter No.	(x, y, z) (m)	Amplitude
1	(−0.08, −0.08, −0.08)	1	5	(0.08, −0.08, −0.08)	1
2	(−0.08, −0.08, 0.08)	1	6	(0.08, −0.08, 0.08)	1
3	(−0.08, 0.08, −0.08)	1	7	(0.08, 0.08, −0.08)	1
4	(−0.08, 0.08, 0.08)	1	8	(0.08, 0.08, 0.08)	1

are increased when SNR is decreased.

From Fig. 3(a) and Fig. 4(a), one can see that the echo data of RSF CSAR are almost like noise, so this will lead to low probability of interception. At the same time, simulation results show that both 2D and 3D targets are well reconstructed, but they are affected by noise level. Therefore, the robustness of CS needs to be improved.

6. CONCLUSION

In this paper, RSF CSAR imaging based on CS is presented. The echo generated by point-target model show that CSAR system is with low probability of interception; the simulation imaging results show that both 2D and 3D point targets are well reconstructed from few samples. Further works on improving the robustness of CS, investigating anti-jamming capability and using other random signal models are underway.

REFERENCES

1. Soumekh, M., *Synthetic Aperture Radar Signal Processing with MATLAB Algorithms*, Wiley, New York, 1999.
2. Bryant, M. L., L. L. Gostin, and M. Soumekh, "Three-dimensional E-CSAR imaging of a T-72 tank and synthesis of its spotlight, stripmap and interferometric SAR reconstructions," *International Conference on Image Processing*, 628–631, 2001.
3. Bryant, M. L., L. L. Gostin, and M. Soumekh, "3-D E-CSAR imaging of a T-72 tank and synthesis of its SAR reconstructions," *IEEE Transactions on Aerospace and Electronic Systems*, Vol. 39, No. 1, 211–227, 2003.

4. Cantalloube, H. M. J., P. Dubois-Fernandez, and X. Dupuis, "Very high resolution SAR images over dense urban area," *IEEE International Geoscience and Remote Sensing Symposium*, Vol. 4, 2799–2802, 2005.
5. Cantalloube, H. and E. C. Koeniguer, "Assessment of physical limitations of high resolution on targets at X-band from circular SAR experiments," *European Conference on Synthetic Aperture Radar,* June 2008.
6. Oriot, H. and H. Cantalloube, "Circular SAR imagery for urban remote sensing," *European Conference on Synthetic Aperture Radar,* June 2008.
7. Palm, S. and H. Oriot, "DEM extraction over urban area using circular SAR imagery," *European Conference on Synthetic Aperture Radar,* June 2008.
8. Frölind, P.-O. U., M. H. Lars, and A. Gustavsson, "First results on VHF-band SAR imaging using circular tracks," *European Conference on Synthetic Aperture Radar,* June 2008.
9. Tan, W. X., Y. P. Wang, H. Wen, et al., "Circular SAR experiment for human body imaging," *Asian and Pacific Conference on Synthetic Aperture Radar*, 90–93, 2007.
10. Tan, W. X., W. Hong, Y. P. Wang, and Y. R. Wu, "A novel spherical-wave three-dimensional imaging algorithm for microwave cylindrical scanning geometries," *Progress In Electromagnetics Research*, Vol. 111, 43–70, 2011.
11. Axelsson, S. R. J., "Random noise radar/sodar with ultrawideband waveforms," *IEEE Transactions on Geoscience and Remote Sensing*, Vol. 45, No. 5, 1099–1114, 2007.
12. Axelsson, S. R. J., "Analysis of random step frequency radar and comparison with experiments," *IEEE Transactions on Geoscience and Remote Sensing*, Vol. 45, No. 4, 890–904, 2007.
13. Candes, E. J., J. Romberg, and T. Tao, "Robust uncertainty principles: Exact signal reconstruction from highly incomplete frequency information," *IEEE Transactions on Information Theory*, Vol. 52, No. 2, 489–509, 2006.
14. Donoho, D. L., "Compressed sensing," *IEEE Transactions on Information Theory*, Vol. 52, No. 4, 1289–1306, 2006.
15. Candes, E. J. and T. Tao, "Near-optimal signal recovery from random projections: Universal encoding strategies?" *IEEE Transactions on Information Theory*, Vol. 52, No. 12, 5406–5425, 2006.
16. Baraniuk, R. and P. Steeghs, "Compressive radar imaging," *IEEE*

Radar Conference, 128–133, 2007.

17. Zhu, X. X. and R. Bamler, "Compressive sensing for high resolution differential SAR tomography-the SL1MMER algorithm," *IEEE International Geoscience and Remote Sensing Symposium*, 17–20, 2010.
18. Wei, S.-J., X.-L. Zhang, J. Shi, and G. Xiang, "Sparse reconstruction for SAR imaging based on compressed sensing," *Progress In Electromagnetics Research*, Vol. 109, 63–81, 2010.
19. Li, J., S. S. Zhang, and J. F. Chang, "Applications of compressed sensing for multiple transmitters multiple azimuth beams SAR imaging," *Progress In Electromagnetics Research*, Vol. 127, 259–275, 2012.
20. Liu, Z., X. Z. Wei, and X. Li, "Adaptive clutter suppression for airborne random pulse repretition interval radar based on compressed sensing," *Progress In Electromagnetics Research*, Vol. 128, 291–311, 2012.
21. Lin, Y., W. Hong, W.-X. Tan, et al., "Compressed sensing technique for circular SAR imaging," *IET International Radar Conference*, April 2009.
22. Chen, S. S., D. L. Donoho, and M. A. Saunders, "Atomic decomposition by basis pursuit," *SIAM Journal on Scientific Computing*, Vol. 20, No. 1, 33–61, 1998.
23. Birgin, E. G., J. M. Martínez, and M. Raydan, "Nonmonotone spectral projected gradient methods on convex sets," *SIAM Journal on Optim.*, Vol. 10, No. 4, 1196–1211, 2000.